Journal of Colloid and Interface Science 652 (2023) 1240–1249

Contents lists available at ScienceDirect

Journal of Colloid And Interface Science

journal homepage: www.elsevier.com/locate/jcis

Tuneable interphase transitions in ionic liquid/carrier systems via voltage control

Sichao Li [a], Georgia A. Pilkington [a], Filip Mehler [a,1], Oliver S. Hammond [b,c], Anthony Boudier [b,2], Alexei Vorobiev [d], Sergei Glavatskih [e,f,g], Mark W. Rutland [a,f,h,i,*]

[a] Division of Surface and Corrosion Science, School of Engineering Sciences in Chemistry, Biotechnology and Health, KTH Royal Institute of Technology, SE-100 44 Stockholm, Sweden
[b] Department of Materials and Environmental Chemistry, Stockholm University, SE-114 18 Stockholm, Sweden
[c] Department of Biological and Chemical Engineering, Aarhus University, Aarhus C 8000 Denmark
[d] Department of Physics and Astronomy, Division of Materials Physics, Uppsala University, SE-751 20 Uppsala, Sweden
[e] System and Component Design, Department of Engineering Design, KTH Royal Institute of Technology, SE-100 44 Stockholm, Sweden
[f] School of Chemistry, University of New South Wales, Sydney, NSW 2052, Australia
[g] Department of Electromechanical, Systems and Metal Engineering, Ghent University, B-9052 Ghent, Belgium
[h] Bioeconomy and Health Department Materials and Surface Design, RISE Research Institutes of Sweden, SE-114 28 Stockholm, Sweden
[i] Laboratoire de Tribologie et Dynamique des Systèmes, École Centrale de Lyon, 69134 Ecully Cedex, France

GRAPHICAL ABSTRACT

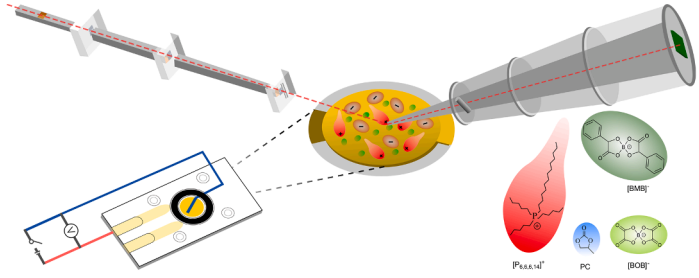

ARTICLE INFO

Keywords:
Non-halogenated ionic liquids
Electric double-layer structure
Interfacial layers

ABSTRACT

The structure and interaction of ionic liquids (ILs) influence their interfacial composition, and their arrangement (*i.e.*, electric double-layer (EDL) structure), can be controlled by an electric field. Here, we employed a quartz crystal microbalance (QCM) to study the electrical response of two non-halogenated phosphonium orthoborate ILs, dissolved in a polar solvent at the interface. The response is influenced by the applied voltage, the structure

Abbreviations: IL(s), ionic liquid(s); EDL, electric double-layer; QCM, quartz crystal microbalance; NR, neutron reflectivity; AFM, atomic force microscopy; PC, 1,2-propylene carbonate; d-PC, 1,2-propylene-d_6 carbonate; $[P_{6,6,6,14}][BMB]$,, trihexyl(tetradecyl)phosphonium-bis(mandelato)borate; $[P_{6,6,6,14}][BOB]$, trihexyl (tetradecyl)phosphonium-bis(oxalato)borate; $[P_{6,6,6,14}]^+$, trihexyl(tetradecyl)-phosphonium cation; $[BMB]^-$, bis(mandelato)borate anion; $[BOB]^-$, bis(oxalato)borate anion; OCP, open circuit potential; SLD, scattering length density; FOM, figure of merit; CV, cyclic voltammetry; WE, working electrode; CE, counter electrode; RE, reference electrode.

* Corresponding authors.
E-mail address: mark@kth.se (M.W. Rutland).
[1] Present address: Department of Physics and Astronomy, Division of Materials Physics, Uppsala University, SE-751 20 Uppsala, Sweden.
[2] Institut Européen de Chimie et Biologie, 2 Rue Robert Escarpit, 33607 Pessac, France.

https://doi.org/10.1016/j.jcis.2023.08.111
Received 22 June 2023; Received in revised form 9 August 2023; Accepted 18 August 2023
Available online 19 August 2023

Quartz crystal microbalance
Neutron reflectivity

of the ions, and the solvent polarizability. One IL showed anomalous electro-responsivity, suggesting a self-assembly bilayer structure of the IL cation at the gold interface, which transitions to a typical EDL structure at higher positive potential. Neutron reflectivity (NR) confirmed this interfacial structuring and compositional changes at the electrified gold surface. A cation-dominated self-assembly structure is observed for negative and neutral voltages, which abruptly transitions to an anion-rich interfacial layer at positive voltages. An interphase transition explains the electro-responsive behaviour of self-assembling IL/carrier systems, pertinent for ILs in advanced tribological and electrochemical contexts.

1. Introduction

Ionic liquids (ILs) are molten salts at relatively low temperatures (T_m < 373.15 K) [1]; their ions are typically large and complex, with delocalized charges, which leads to inhibition of their ability to crystallize [2]. Due to their generally high chemical and thermal stability, low melting points, and negligible volatility [3], ILs have been extensively studied in many energy applications, such as fuel and solar cells, supercapacitors and electrochemical devices, and enhanced efficiency of lubrication technologies [4–7]. Due to their ionic nature, external electrical fields can alter the interfacial structures and interfacial characteristics of ILs (*e.g.,* their friction behaviour), making them promising for improving energy efficiency with additional functionality [8–10]. Several issues have hampered the commercial application of ILs, including high production costs, poor miscibility in common base fluids (*e.g.,* mineral oil), and problems associated with the widespread use of fluorine-containing anions, which produce toxic and corrosive halogen halides under tribological conditions (*i.e.,* high temperatures and pressures) [11,12]. We henceforth refer to the Fluorinated Anion Ionic Liquids as FAILs.

To address these issues, a series of non-halogenated ILs were synthesized and developed [13,14], which show promising potential both as neat lubricants [15] and as additives [16,17]. In particular, non-halogenated ILs containing phosphorus- and boron-based ions show enhanced thermal stability and anti-wear capacity [18]. The chelated orthoborate anion can generate a tribo-chemical thin film due to physicochemical adsorption, which lowers shear strength at the interface, reducing friction [11,19]. Long alkyl chain phosphonium cations offer advantages over other cation architectures (*e.g.,* ammonium, imidazolium cations) due to their stability and capability to form a surface-protective film in boundary and mixed lubrication regimes [20,21]. Additionally, the excellent electro-responsive property of ILs allows active control of advanced lubrication systems using electric fields, so-called “tribotronics” [22]. However, to fully exploit the tribological performance of ILs, a better understanding of the effect of electric fields on the interfacial structure and composition control in neat ILs or IL-in-carrier systems, as well as the intimate relationship between their structures and tribological properties, is required.

At an electrified surface, ILs mainly manifest in the interfacial region as an electric double-layer (EDL), the nature of which remains an active topic of research due to the complex ion ordering [23]. Bazant *et al.* proposed a phenomenological theory to describe EDL structure at charged interfaces, *i.e.,* overscreening and crowding structures [24]. Both experiment and simulation studies have proved this theory [25–28]. In other cases, such as short chain imidazolium-based ILs, the cation and anion coexist at charged interfaces in a checkerboard ion arrangement [29]. Furthermore, certain ILs with amphiphilic (*i.e.,* long alkyl chains) structures can self-assemble into lamellar-like bilayer interfacial structures [30–33], rather than coulombic-dominated arrangements.

Previous approaches to characterize the interfacial structures and self-assembly of ILs (or ILs in the carrier) systems have included experimental techniques, such as electrochemical impedance spectroscopy (EIS) [34,35], quartz crystal microbalance (QCM) [36,37], sum-frequency generation (SFG) spectroscopy [32], atomic force microscopy (AFM) [9,38–42], surface force apparatus (SFA) [43], X-ray (XRR) [44], small-angle neutron scattering (SANS) [45] and neutron reflectivity (NR) [46,47], as well as molecular dynamics (MD) simulations [48]. Previously, we have investigated the electro-responsive composition and structure of one non-halogenated IL, trihexyl(tetradecyl) phosphonium-bis(mandelato)borate [$P_{6,6,6,14}$][BMB] on an electrified amorphous gold surface, both as a pure IL and when dispersed in a polar solvent (*e.g.*, lubricant base oil, acetone, propylene carbonate), using QCM, NR, AFM, among other techniques [37,39,47,49]. Nano-tribological AFM measurement can study modulated IL boundary layers at different potentials which enable an electroactive friction reduction [49]. In the case of QCM, the minute changes in interfacial mass associated with the ion exchange of IL dissolved in a polar oil as a function of potential can be probed by monitoring the resonance frequency change of the gold-coated quartz crystal [37]. Meanwhile, NR has shown distinct advantages in providing interfacial structural information for such IL/carrier systems, which is relatively challenging to decouple solely using QCM [47]. In neutron studies particularly, irreversible effects could sometimes be observed at higher positive potentials, which were then interpreted as electrochemical damage and led to the electrochemical window being drastically reduced. Given the documented electrochemical stability of the ILs in question, further investigation into this unusual phenomenon led to the current work, where a novel interpretation is proposed.

Here, we have used both QCM and NR measurements in parallel to investigate the electro-responsive interfacial composition and structure changes of another IL, trihexyl(tetradecyl)phosphonium-bis(oxalato) borate ([$P_{6,6,6,14}$][BOB]), dispersed in the polar aprotic solvent propylene carbonate (PC). This IL has the same cation as previously studied [$P_{6,6,6,14}$][BMB] (to which its QCM electro-responsivity is also compared herein), but the $[BOB]^-$ anion is considerably smaller. PC is selected as the solvent because of its high dielectric constant and low viscosity, making it a suitable charge carrier. Deuterated PC has a high scattering length density (SLD), allowing the possibility of contrasting the bulk solution with that of the gold electrode in NR measurements. In this paper, we will therefore use QCM and NR to provide clear evidence that electric fields affect the interfacial composition and structure of IL/carrier systems and suggest a voltage-induced interphase transition of [$P_{6,6,6,14}$][BOB] from a self-assembled bilayer structure to the usual EDL structure. This finding supports the above-mentioned feature at higher positive potentials, and also has important ramifications for the reversibility of controlled interfacial structures, which is required for supercapacitors and “red button” like control of friction in tribotronic applications [50].

2. Materials and methods

2.1. Materials and solution preparation

The ILs trihexyl(tetradecyl)phosphonium-bis(mandelato)borate [$P_{6,6,6,14}$][BMB] and trihexyl(tetra-decyl)phosphonium-bis(oxalato) borate [$P_{6,6,6,14}$][BOB] (cf. Fig. 1) were synthesized at Luleå University of Technology and used without further purification. The high purity of the ILs was confirmed using mass spectroscopy elemental analysis and multinuclear nuclear magnetic resonance (NMR) spectroscopy. Water content was tested by Karl Fischer titration, and was found to be 0.033 wt% and 0.06 wt% for [$P_{6,6,6,14}$][BMB] and [$P_{6,6,6,14}$][BOB],

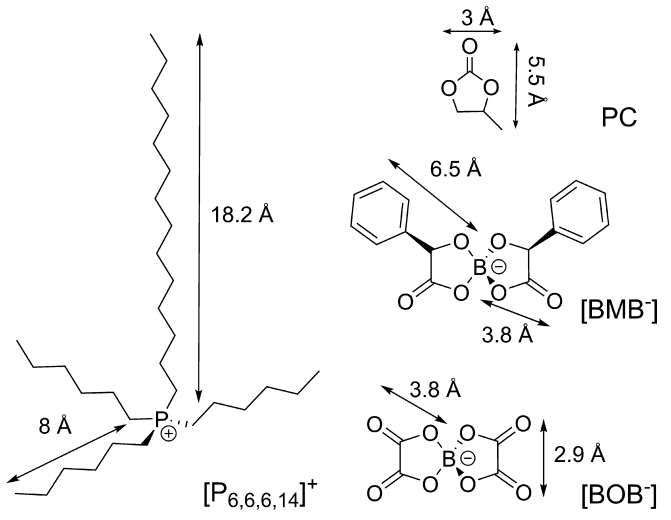

Fig. 1. Molecular structures and dimensions of IL ions and the solvent, PC.

respectively [13,14]. Before the solutions were prepared, the pure ILs were baked under vacuum at 60 °C for ~ 72 h to remove any traces of solvent and the residual water. The solvents 1,2-propylene carbonate (PC, anhydrous, 99.7%, Sigma Aldrich) and 1,2-propylene-d_6 carbonate (d-PC, 99.5 atom% D, Qmx Laboratories Ltd.) were used as received. The IL/PC solutions were prepared by weighing the corresponding IL and adding the appropriate volume of solvent. In this paper, the concentration of the solution is presented in terms of weight percentage (% w/w). For the measurements presented here, both $[P_{6,6,6,14}][BMB]$/PC and $[P_{6,6,6,14}][BOB]$/PC concentration is 20% w/w, corresponding to 3.1 mol% and 3.9 mol% of the IL, respectively. Each solution was ultrasonicated for at least 10 min until homogeneous (by visual assessment) to ensure complete mixing and was used immediately.

For NR measurement, the bulk SLD of $[P_{6,6,6,14}][BOB]$/PC 20% w/w solution was contrast matched to (or as close as possible to) that of gold (4.56×10^{-6} Å^{-2}) by utilizing deuterated PC (cf. Table 1). The solutions were characterized with Fourier-transform infrared spectroscopy (FT/IR-4600, fitted with a single-reflection ATR accessory, Jasco) before and after the NR measurement to determine the stability and water content of the IL solution. The IR spectra for the $[P_{6,6,6,14}][BOB]$/PC 20% w/w solution used for the NR measurement are provided in the Supplementary Information (cf. Figure S1) and did not exhibit any distinguishable water peaks.

2.2. Quartz crystal microbalance

An A100® QCM (Attana AB, Sweden) was used with a custom-built electrochemical cell experiment setup for the frequency potential measurements. 10 MHz quartz crystals and the QCM sensor chip were also provided by Attana AB. The crystals were sputtered with a 150-nm thick gold layer and used as a working electrode (WE). The quartz crystal wave velocity and density were 3340 m/s and 2650 kg/m^3, respectively.

Table 1
Densities, molecular volumes and SLDs of IL ions and solvent.

Species	ρ at 25 °C (g/cm^3)	V_M (Å^3)	SLD ($\times 10^{-6}$Å^{-2})
$[P_{6,6,6,14}][BOB]$	0.997	1118	0.37
$[P_{6,6,6,14}][BMB]$	1.023	1291	/
$[P_{6,6,6,14}]^+$	0.878	914	−0.40
$[BOB]^-$	1.521	204	3.84
$[BMB]^-$	1.376	378	/
h-PC	1.205	141	/
d-PC	1.258	143	5.87

Note: The SLD for $[P_{6,6,6,14}][BMB]$, $[BMB]^-$ and h-PC are not relevant to this study.

To facilitate electrochemical measurements, the components of the supplied QCM sensor chip were modified by cutting small recesses in the cell lid and holder to accommodate a Pt wire (⌀ = 0.15 mm), which was used as a counter (CE) and quasi-reference electrode (RE). The QCM crystal is sealed by an FFKM X-ring (internal ⌀ = 6.07 mm Trelleborg, Sweden), which is accommodated by a recess in the cell lid. A custom-built potentiostat [36,37] was used to apply different potentials across the cell. An insulated copper wire connected the Pt wire with the battery circuit. Two multimeters (3000 FC series, FLUKE) were used during all experiments to monitor the applied potential across the cell and open circuit potential (OCP) decay. The experimental setup is described in detail elsewhere [36,37]. The QCM cell components (except the crystal) were ultra-sonicated for 30 mins in a 2% v/v solution of Deconex Universal (VWR, UK) with Milli-Q water (resistivity 18.2 MΩ cm at 25 °C; total organic carbon (TOC) ≤ 5 ppb), then rinsed thoroughly with Milli-Q water and finally absolute ethanol before drying with filtered nitrogen. The QCM crystals were soaked in a 2% v/v solution of Deconex Universal in Milli-Q water for 30 min before rinsing and drying with the same procedures as above.

IL solutions were injected using a syringe via one of the holes in the chip lid. After mounting in the QCM, the system was stabilized overnight to reduce the intrinsic drift (<1 Hz/min). The temperature of the system during experiments was maintained at 25 °C. Before applying the potentials, the OCP under "initial unperturbed condition" was measured across the QCM cell. The OCP average values for 20% w/w $[P_{6,6,6,14}][BMB]$/PC and 20% w/w $[P_{6,6,6,14}][BOB]$/PC were −0.32 V *vs* Pt, and −0.16 V *vs* Pt, respectively. For each measurement, a potential was applied for 5 min. After turning off the applied potential, the OCP decay was recorded for approximately 2–5 mins, depending on the decay rate. The frequency was monitored throughout the whole experiment. For each of the curves corresponding to a potential response, the frequency change is with respect to the intrinsic drift baseline value immediately prior to the voltage change. In general, the largest potential was applied first, and the next applied potential was the same magnitude with opposite bias, then cycled to the second largest potential, and so on. This specific sequence is designed to facilitate the re-establishment of the baseline. The applied potential region was −0.8 V to +0.8 V, with a decrement of 0.2 V. Before changing the different potentials, the setup was allowed to fully relax for at least 20 min until the OCP decay equilibrated close to zero, and the baseline of the intrinsic drift was re-established. Note that the Attana program returns the frequency *reduction* value resulting in a positive frequency change with a positive mass increase (overall frequency reduction), which is intuitively more convenient. Sauerbrey's equation [51] was used to convert measured frequency changes to mass changes in $ng \bullet cm^{-2}$, which has been shown to be a reasonable assumption for electroresponsive measurements where the bulk conditions are unchanged [36,37].

2.3. Neutron reflectivity measurements and analysis

The NR measurements for 20% w/w $[P_{6,6,6,14}][BOB]$/PC were performed using a custom-made electrochemical NR cell. The details of the cell design have been reported previously in the related studies for $[P_{6,6,6,14}][BMB]$ in acetone and PC systems [47,49]. Briefly, a thin (~170 Å) amorphous gold film was deposited on a 10 mm (50 × 50 mm) polished silicon (1 0 0) block (Sil'tronix Silicon Technologies, Archamps, France) and used as the working electrode (WE). A thin chromium (Cr) layer was pre-coated on the silicon surface as an adhesion layer. The NR measurement was first performed for the gold-coated block in air to characterize the Si, SiO_2, Cr, and Au layer parameters (*i.e.,* SLDs, thickness and roughness), which were used as references for the subsequent IL solution NR fitting. (cf. Figure S2 and Table S1).

A short insulated copper wire was adhered to one corner of the gold surface with conductive epoxy (CW400, Chemtronics), which was cured in an oven at 120 °C for 20–30 min. After cooling down from the oven, the gold surface was rinsed with filtered absolute ethanol, blown dry

with nitrogen, and exposed to UV/ozone for 10 min to remove any organic residues. A conductive glass (coated with fluorine-doped tin oxide, FTO, Sigma Aldrich) was chosen as the counter/reference electrode (CE/RE). For the measurement presented here, we chose a two-electrode system due to the limited space for the cell configuration. A PTFE gasket of 0.5 mm thickness was used to separate the CE/RE from the WE and to contain the IL solution. Before assembling the NR electrochemical cell, the conductive glass, gasket, and all other cell components were ultra-sonicated in 2% v/v Hellmanex® for 30 min at room temperature, followed by rinsing thoroughly with Milli-Q water and filtered absolute ethanol, before finally blowing dry with nitrogen. To minimize ambient water contamination, the cell was assembled inside a polyethylene glove bag under a dry argon atmosphere (R.H. $<$ 10%). The IL solution was injected into the cell with the adapter using a glass Luer syringe. After mounting the cell on the beamline, electrical potentials were applied across the cell with a potentiostat (Metrohm Autolab, PGSTAT204). The applied electrical potentials were chosen based on the measured stable electrochemical window, demonstrated by the cyclic voltammetry (CV) pre-tests (offline). The OCP for 20% w/w $[P_{6,6,6,14}]$[BOB]/PC was measured as −0.42 V *vs* FTO before applying the potentials. In comparison, the OCP of NR cell for 20% w/w $[P_{6,6,6,14}]$[BMB]/PC is referred to as −0.05 V *vs* FTO in our previous work [49]. The potentials were applied in the same order as presented. Before the NR measurement, the cell was stabilized under each applied potential for 30 min to reach equilibrium. The applied potential and current across the cell were continuously recorded and monitored during all NR measurements (cf. Figure S3). After all the NR tests, additional CV measurements were performed across the IL/carrier solution in the electrochemical NR cell again to examine whether any Faradaic events had occurred during the NR measurements and determine the charge transfer reversibility [47]. The CV measurements for 20% w/w $[P_{6,6,6,14}]$[BOB]/PC before and after NR experiments can be found in the supplementary material (cf. Figure S4).

The NR measurements presented here were performed on the SuperADAM reflectometer at the Institut Laue-Langevin (ILL), Grenoble, France [52]. The neutron specular reflectivity R (the ratio of intensity between the reflected and the incident beam) was measured as a function of the momentum transfer vector, $Q_z = \frac{4\pi}{\lambda}\sin\theta$, where λ is the wavelength and θ is the angle of incidence. During the measurement, the wavelength was fixed at 5.21 Å, and the angle of incidence was varied, providing a Q_z-range of 0.005–0.21 $Å^{-1}$. For the solution NR measurement, the neutron beam was directed through the Si block, reflected from the gold-solution interface, before again traversing the block and exiting towards the detector. All the original scattering data were reduced according to the standard procedures of SuperADAM, using the program pySAred. These procedures include background subtraction, detector efficiency calibration, direct beam normalization and over-illumination correction [49].

The reduced data were fitted with the software package GenX [53,54], using a slab model in which the layer's thickness, roughness and SLD are constrained between super- and subphases [55,56]. The substrate parameters of the Cr and SiO_2 layers (*i.e.*, SLD, thickness, and roughness) were obtained from the reflectivity of the block measured in air (cf. Table S1) and fixed for all subsequent potentials. Gold layer thickness and the bulk SLD were fitted for the first applied potential (*i.e.*, 0 V) and fixed for the subsequent potentials. Additionally, a "micro-slabbing" approach [57] was applied for the gold-IL ion interfacial region fitting due to the gold layer roughness being comparable to the IL's molecular dimensions (cf. Fig. 1). This approach sliced the gold-1st IL ion layer interfacial region into a series of 1 Å thick slabs of 0 Å roughness. The SLD of every micro-slab is determined based on the normal distribution of the volume fraction of gold and 1st IL ion layer, which can describe a smooth transition in this region. Instead of the interfacial gold roughness, the thickness of this interfacial region can be fitted and fixed after the first applied potential [58]. Apart from these, the SLD of the interfacial layers, as well as the roughness of the IL/bulk interfaces, were allowed to vary for all the fitted datasets.

A single-layer slab model was used initially for fitting, and subsequent layers were only invoked if the logarithmic figure of merit (FOM) value decreased. For each simulation of different potentials, no predefined interfacial structures were assumed. The layer SLDs were constrained to be in the range of the possible component species. The estimated SLD of $[P_{6,6,6,14}]$[BOB] was calculated from its measured mass density (0.997 g/cm^3 at 25 °C) using an Anton Paar density meter (DMA^{TM} 4500 M). The densities, molecular volumes and SLDs of ions are listed in Table 1, where the density and molecular volume of ions were calculated from atomistic simulations [37]. The SLD profiles were obtained from the best fits of the NR data, determined by the lowest logarithm of the FOM value with the minimum number of layers.

3. Results and discussion

3.1. Quartz crystal microbalance

QCM has a high mass sensitivity towards solution-surface interfacial changes; it can detect mass changes corresponding to less than a monolayer [59]. Thus, by monitoring the changes in frequency, QCM can be used to study the effects of ion exchange and potentially reveal the nature of the rearrangements and the various structures (*e.g.*, over-screening or checkerboard) at the solid–liquid interface [37]; it is impossible to obtain the precise amount of IL in the film (a more conventional use of QCM), rather, the measurements reveal the *changes* in the film due to the effects of electric potential. Fig. 2 shows the resonance frequency change as a function of time with different potentials for the 20% w/w $[P_{6,6,6,14}]$[BMB]/PC and the 20% w/w $[P_{6,6,6,14}]$[BOB]/PC solutions. Upon polarisation of the gold surface (*i.e.,* under applied potentials), the IL/PC solutions showed an abrupt *initial* response and a subsequent gradual decay towards a *plateau* value. Both the initial response and plateau value change as a function of the magnitude of the applied potentials and typically show opposite dependences on the potential sign. The physical meaning of these two features is analyzed separately below.

The abrupt *initial* frequency change values are plotted as a function of applied potentials in Fig. 3 for the reference PC system and the two 20% w/w IL solutions. Both the PC and the $[P_{6,6,6,14}]$[BMB] solution display a linear response with the potential, with the PC having a slightly stronger dependence. Due to its large dipole moment, a net response in PC orientation to the applied potential is expected. In a molecular dynamic (MD) simulation study, PC was found to be plentiful in the IL solution's EDL and altered its molecular orientation at different potentials on an electrified graphite surface [60]. It seems likely that the high sensitivity of QCM allows these orientational changes to be detected as a slight change in the resonant frequency. The abruptness of this change reflects the small size of the PC molecules and their ability to rapidly adapt to the local electric field. The comparable linear behaviour of the $[P_{6,6,6,14}]$[BMB] system indicates a similar solvent response. This in turn suggests both that there is significant solvent in the $[P_{6,6,6,14}]$[BMB] interfacial film, and that the applied electric field is not as screened by the presence of ions at the interface. For the $[P_{6,6,6,14}]$[BOB] solution, this solvent response is undetectable at negative potentials and very weak at positive values. The value at +0.8 V was masked by the very different behaviour in that case (cf. Fig. 2d) and could not be extracted. It is likely the consequence of structural changes, which will be discussed in more detail later. A possible reason for this apparent difference is that the smaller size of $[BOB]^-$ anions, compared with $[BMB]^-$ (cf. Fig. 1), allows them to pack more efficiently at the interface together with any (self-assembled) cations, and results in less PC being present at the electrode interface. The reduced response also reflects the greater charge dissociation of the $[P_{6,6,6,14}]$[BOB] in a polar medium [16], which alters both the absolute amount of IL in the interfacial film and how much the electric field is screened.

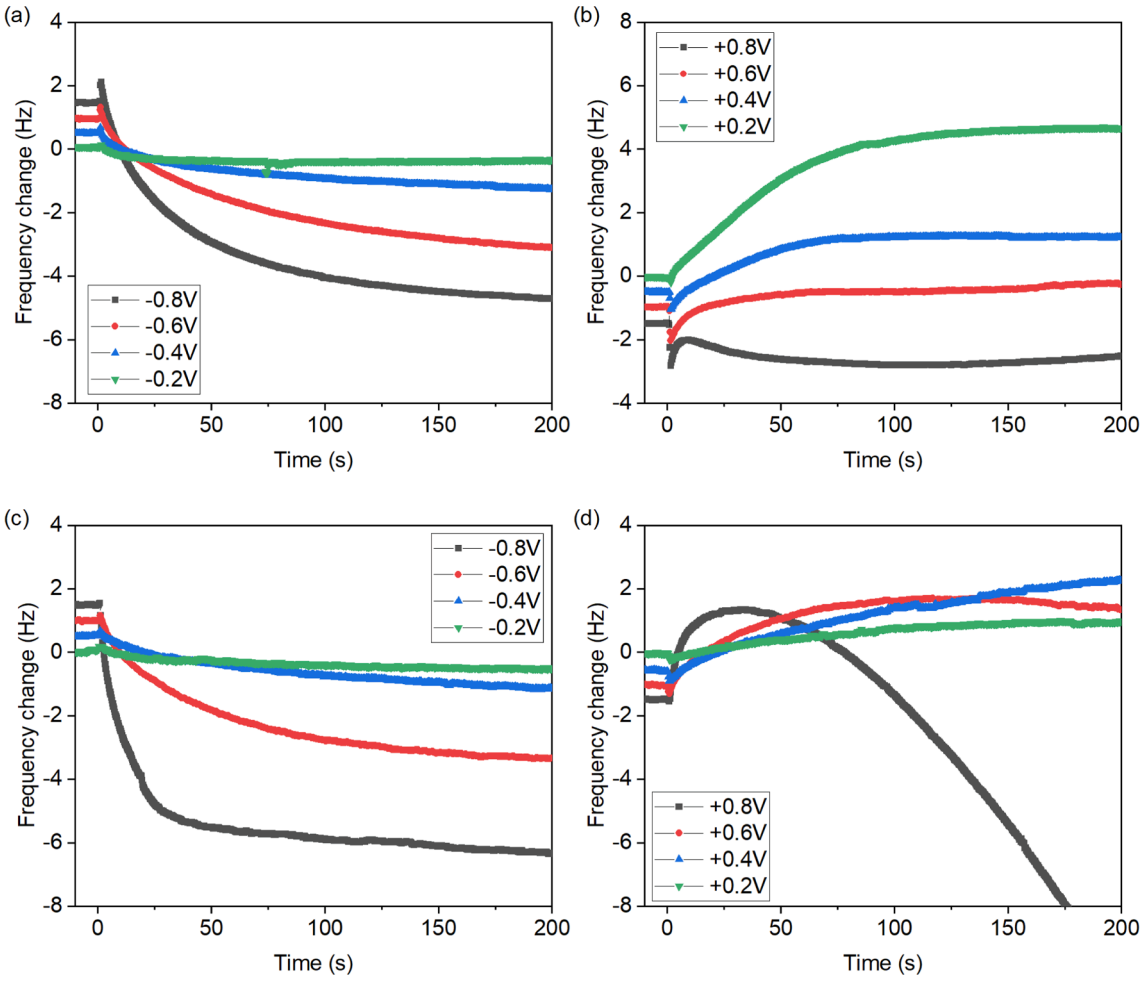

Fig. 2. QCM resonance frequency changes as a function of time for 20% w/w $[P_{6,6,6,14}][BMB]/PC$ with negative potentials (a) and positive potentials (b), and 20% w/w $[P_{6,6,6,14}][BOB]/PC$ with negative potentials (c) and positive potentials (d). For clarity, the curves are offset by 0.5 Hz from each other on the y-axis.

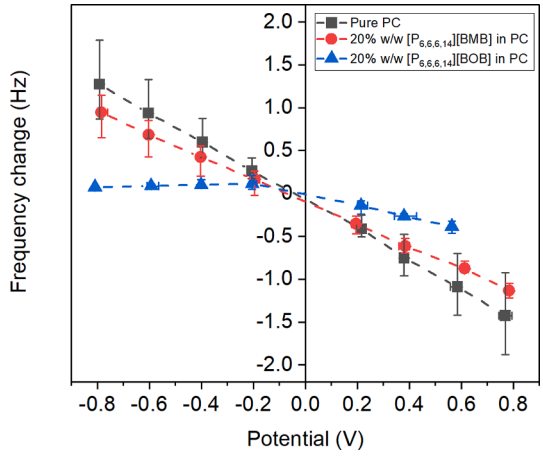

Fig. 3. Initial frequency change with different applied potentials for pure PC, 20% w/w $[P_{6,6,6,14}][BMB]/PC$ and 20% w/w $[P_{6,6,6,14}][BOB]/PC$. The error bars represent the data's maxima and minima values for three independent experiments.

The second feature observed in Fig. 2 was a more gradual decay with time towards a *plateau* to achieve a frequency (or mass) change of the opposite sign to the solvent response. This second more significant and prolonged response is due to changes in the composition and structure of the ionic layers close to the polarized gold surface [36]. The frequency values of the plateaus were transformed into mass changes using Sauerbrey's equation [51]. As mentioned above, while Sauerbrey's equation is strictly for elastically bound layers, this approximation has been shown to be valid [37], since the viscosity and density of the medium do not change, only the composition of the adsorbed film changes. These mass changes are subsequently plotted as a function of applied potentials in Fig. 4. Notably, these changes reflect the *change* in mass at the electrode for each system and reveal nothing about the solvent content, film structure and so on, which may be very different, as is in fact implied by the data in Fig. 3. At negative potentials, the results broadly show a decrease in mass for the IL systems, reflecting the different densities of the molecules (density sequence: $\rho_{cation} < \rho_{IL} < \rho_{PC} < \rho_{anion}$, *cf.* Table 1), and is consistent with a slight increase in the number of (less dense) cations relative to anions at the interface, as co-ions (*i.e.,* $[BMB]^-$ or $[BOB]^-$ anions) are effectively expelled in response to the negative potential [37]. At positive potentials, both 20% w/w $[P_{6,6,6,14}][BMB]/PC$ and 20% w/w $[P_{6,6,6,14}][BOB]/PC$ systems show a non-symmetrical and complex variation, which points at a different mechanism that will be discussed in more details later.

The 20% w/w $[P_{6,6,6,14}][BMB]/PC$ results show the two consequences of using larger $[BMB]^-$ anions. Firstly, as implied in Fig. 3 and from neutron reflectometry experiments [49], the interfacial layer has a higher solvent content. Secondly, the self-assembly is constrained, and there is a greater degree of ion-pairing with $[P_{6,6,6,14}]^+$ cations (*i.e.,* a lower degree of dissociation), resulting in the dominant structure of the EDL being an intrinsically checkerboard interfacial structure (cf. Fig. 5**b-d**), but one where the number of cations and anions in the first layer

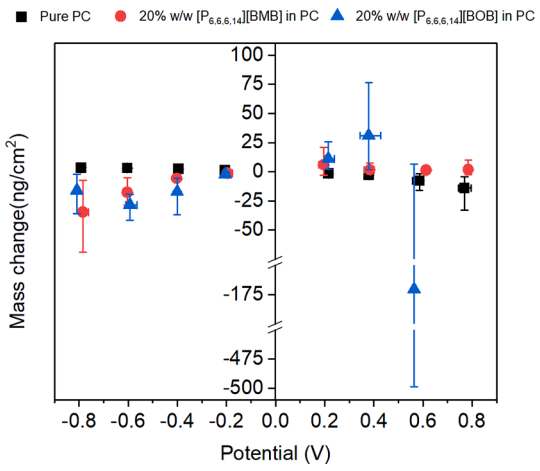

Fig. 4. QCM mass changes as a function of applied potentials for pure PC, 20% w/w $[P_{6,6,6,14}][BMB]$/PC and 20% w/w $[P_{6,6,6,14}][BOB]$/PC. For clarity, the mass change for 20% w/w $[P_{6,6,6,14}][BOB]$/PC at the largest positive potential (~0.8 V) is excluded, which is shown in the supplementary material (cf. Figure S5). The error bars represent the data's maxima and minima values for three independent experiments (cf. Table S2).

varies systematically in response to the surface charge. (The number of "dark and light squares" changes with the surface potential to retain the analogy.) As was described in the preceding paragraph, a negatively polarized surface would expel both $[BMB]^-$ anions and potentially even polarized PC molecules, and fill the resulting void with cations or $[P_{6,6,6,14}][BMB]$ ion pairs from the solution, either or both of which would tend to reduce the interfacial region mass. However, the mass change with the sign of the charge is not symmetrical; the equivalent argument for the displacement of cations (and possibly PC), with replacement by intermediate-density IL ion pairs, would largely nullify the mass change at positive potentials. This explains our observation of the less pronounced mass change for $[P_{6,6,6,14}][BMB]$/PC in the positive region. This argument is also supported by previous neutron data, which is consistent with the replacement of cations with ion pairs [49], although this argument was not explicitly discussed.

The situation becomes much more complicated for 20% w/w $[P_{6,6,6,14}][BOB]$/PC. While the mass changes at negative potentials are comparable (bear in mind that *changes* are observed, and this does not mean the layers need to have similar structures or densities), the behaviour at positive potentials is significantly different. The ion-exchange density difference approach works well at negative and small positive potential regions (−0.8 V to +0.4 V), where the denser $[BOB]^-$ anions (and possibly polarized PC) are expelled and their volume formally replaced by neutral IL ion pairs, leading to a reduced mass for negative potentials and a mass increase with positive potentials (*i.e.,* sparser $[P_{6,6,6,14}]^+$ cations exchanged by IL ion pairs). There is a dramatic change in behaviour at intermediate to large positive voltages, with an opposite trend, rendering this approach inapplicable (cf. Fig. 4). A pronounced negative mass change is observed in all repeated measurements. Note that the error bars appear large in this area as a result of averaging three curves that all change very steeply; the trend is reproducible (cf. **Table S2**), but the transition point varies by a few mV. This slight variation is possibly due to tiny differences in the placement of the electrodes (*i.e.,* WE-CE distance) or the voltage history (the exact time and value of each applied potential were not rigidly controlled). A new explanation for this anomalous mass change must be sought, which considers the molecular architectures and ion packing behaviours.

In some recent studies, amphiphilic ILs with long alkyl chains on one of the ions have been shown to self-assemble into bilayer structures at electrified surfaces [32,61–63]. Because of the smaller structure of $[BOB]^-$ anions and high dissociation of the IL ions (with consequent relative independence and mobility) [16], the $[P_{6,6,6,14}]^+$ cations are more likely to form a bilayer structure at the electrified surface, at least at negative potentials, which can be thought of as a self-assembly modified Coulombic crowding phenomenon [45]; this behaviour is uncharacteristic of more conventional, non-self-assembling ILs. At negatively and weakly positively polarized (up to ~ 0.4 V) surfaces, the polar heads of the $[P_{6,6,6,14}]^+$ cations are electrostatically attracted to the interface. The non-polar tails orientate outward, close to the non-polar tails of a subsequent $[P_{6,6,6,14}]^+$ cation layer, thus forming a bilayer at the interfacial region (in the "surfactant-like" sense of the word, cf. Fig. 5**e-f**). At sufficiently high positive external voltages, the bilayer structure of cations becomes untenable as the cation density becomes too low to support a self-assembly structure (cations are repelled). This necessarily induces an interphase transition to a more energetically favoured EDL arrangement, *i.e.*, a coulombically ordered checkerboard structure (cf. Fig. 5**g**). It should be noted that the transition occurs at positive polarity, resulting in more anions in the layer. As such, referring to it as an "anion-rich interfacial layer" may be more appropriate. This interphase transition from a highly dense bilayer structure to a more sparsely populated, and thinner EDL structure should indeed result in a dramatic mass reduction at higher positive voltages. However, it is not sufficient to infer the above hypothesis from the QCM interfacial mass change alone; it is desirable to provide complementary evidence using other techniques to verify such phenomena. Neutron reflectometry, for example, is one of the few techniques capable of directly supporting this argument, as demonstrated in the ensuing section.

The frequency data from the QCM provides a measure of the

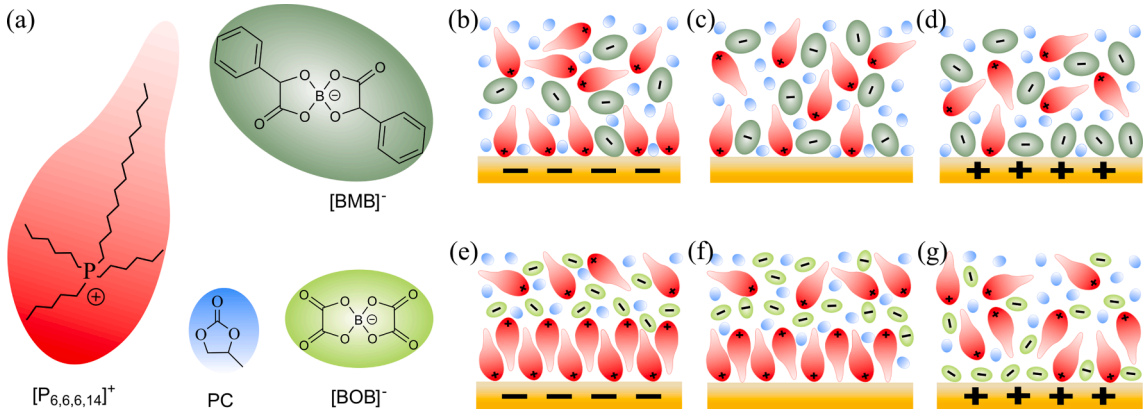

Fig. 5. Proposed model for the EDL of two IL/PC systems on electrodes as a function of the potential. (a) The schematics for different molecules. (b-d) for 20% w/w $[P_{6,6,6,14}][BMB]$/PC system. (e-g) for 20% w/w $[P_{6,6,6,14}][BOB]$/PC system. These cartoon schematics are not to scale, but to aid visualization of the molecular structures. For the actual size of the molecules, please refer to Fig. 1.

changing surface charge of the IL interfacial layer. An independent measure of the change in charge can be obtained by monitoring the potential externally as the system relaxes to OCP. After disconnecting the external potential to the QCM cell, the OCP was thus monitored to investigate the capacitive effect of the system. In a previous study, it was demonstrated that the OCP decay of a neat IL or IL as an additive is consistent with a diffusive discharging capacitor behaviour, according to **Equation (1)** [36,37]:

$$V = V_0 \cdot \exp[-\frac{\sqrt{t}V_0}{RQ_0}] \quad (1)$$

where V_0 is the initial applied voltage, R is the resistance, and Q_0 is the initial charge density where $C_0 = Q_0/V_0$,

Fig. 6 shows a representative graph where the decaying OCP is plotted as a function of $t^{1/2}$ for 20% w/w $[P_{6,6,6,14}][BOB]$/PC solution with negative applied potentials. However, it is challenging to fit the data points to an exponential in the present case (**Equation (1)**), due to the initial sharp decay in potential curves, particularly for high voltages (cf. Fig. S6**a**). This sharp decay is inconsistent with the ideal, single-component capacitor behaviour which was observed for neat IL [36], which might be caused by the lower conductivity of the solvent (PC), raising the resistance to the capacitive current across the cell, leading to an additional capacitive voltage drop. At high voltages (especially for +0.8 V), the deviation from the exponential fit caused by the solvent term is clear. Equation (1) thus needs to be modified to take this additional solvent capacitive term into account for high voltages (±0.4 V to ±0.8 V):

$$V = A_0 + V_0 \cdot \exp[-\frac{\sqrt{t}V_0}{RQ_0}] \quad (2)$$

A value for the capacitance charge, extracted from the value of the fitted exponential constant and the applied potential [36], can be re-plotted as a function of applied potential. In Fig. 7, this capacitance charge has arbitrary units because the resistance is unknown. The agreement between the values obtained for the two systems is striking, but expected since the system is 80% PC in both cases. The figure reveals a rather linear relationship for the $[P_{6,6,6,14}][BMB]$/PC system, as predicted for classical capacitive behaviour. However, the capacitive behaviour deviates from a linear relationship at the voltage extremes for the $[P_{6,6,6,14}][BOB]$/PC system (cf. Fig. 7 +0.6 V, +0.8 V). The dramatic changes in the apparent mass for the $[P_{6,6,6,14}][BOB]$/PC system are not reflected here since the capacitive charge is expected to be independent of the interfacial structure; the system adopts a structure that minimizes the energy, and the charge of the interfacial region is given by the ratio

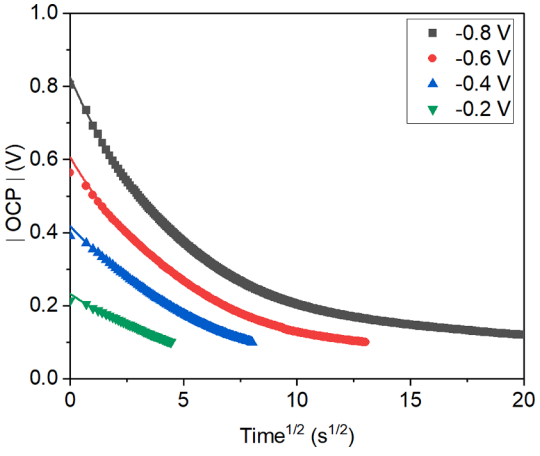

Fig. 6. OCP relaxation as a function of $t^{1/2}$ for different negative potentials of 20% w/w $[P_{6,6,6,14}][BOB]$/PC. The symbols represent experimental data, and the solid lines represent the improved fits for the data using **Equation (2)**.

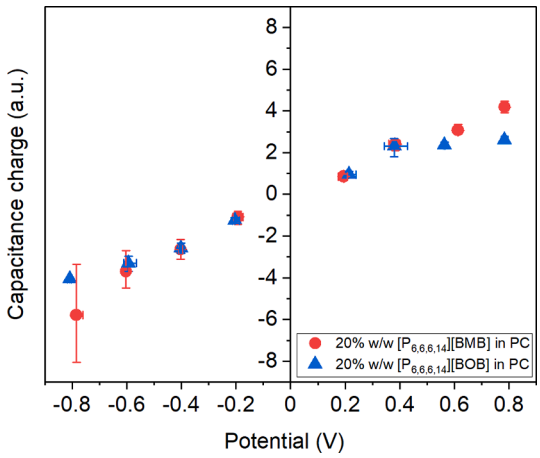

Fig. 7. Calculated capacitance charge as a function of applied potentials for 20% w/w $[P_{6,6,6,14}][BMB]$/PC and 20% w/w $[P_{6,6,6,14}][BOB]$/PC. The error bars represent the data's maxima and minima values for three independent experiments.

of anion and cations at any voltage. Nonetheless, the deviation in the $[P_{6,6,6,14}][BOB]$/PC system likely reflects a higher IL content in the interfacial region (consistent with the results of Fig. 3).

3.2. Neutron reflectivity

Neutron reflectometry is one of the few techniques that provide information on the z dependence of the ion distributions (*i.e.,* the variation in chemical composition with distance from the surface). The intrinsic sensitivity of neutrons to nuclei is a well-known and unique trait that can be leveraged to increase or decrease the contribution of their scattering from different portions of the solution by selecting materials with considerably different SLDs or substituting different isotopes. With a suitable selection of the SLDs of the surface, interfacial layer and solution, it is thus possible to obtain insight into the distribution of species far from the surface. The SLD of the bulk solution was contrast matched to that of gold, using deuterated PC (d-PC, SLD = 5.87×10^{-6} Å^{-2}) to enable sensitive probing of any changes to the interfacial region. Due to the difference of SLD between the component ions, the changing SLD upon ion exchange at the electrified surface can provide information regarding the composition of the interfacial layer(s), as well as their thickness [47].

Fig. 8**a** shows the NR curves for the 20% w/w $[P_{6,6,6,14}][BOB]$ in d-PC at a gold electrode surface for three different potentials (0 V, −1.5 V, +0.5 V). The pronounced Kiessig fringes indicate a strong SLD contrast between the interfacial region and the gold electrode. The NR profile would be featureless if no structured layers were present at the gold interface. With applied potentials, the changes in the *positions* of the Kiessig fringe maxima and minima indicate the changing thickness of the interfacial layers. The variation in the Kiessig fringe *amplitude* signifies the change of SLD at the gold-IL solution interface. For the positive potential (+0.5 V), there was a slight shift towards higher Q and reduced amplitudes in the Kiessig fringes, suggesting a more diffuse interfacial layer with less SLD contrast to the gold electrode. The reflectivity difference for both polarized potentials (with respect to 0 V) was calculated and is shown as asymmetry plots in Fig. 8**a** inset. For both positive and negative potentials, an oscillatory function was observed across the whole Q_z range, suggesting a systematic electro-responsivity of the IL at the gold interface.

The SLD profiles corresponding to the best fit to the reflectivity curves as a function of the distance from the gold surface (z = 0) are shown in Fig. 8**b**. The solution SLD could not be perfectly matched to the gold due to the lower SLD of the dissolved IL, as seen from the SLD profiles in Fig. 8**b** derived from fitting the curves in Fig. 8**a**. With

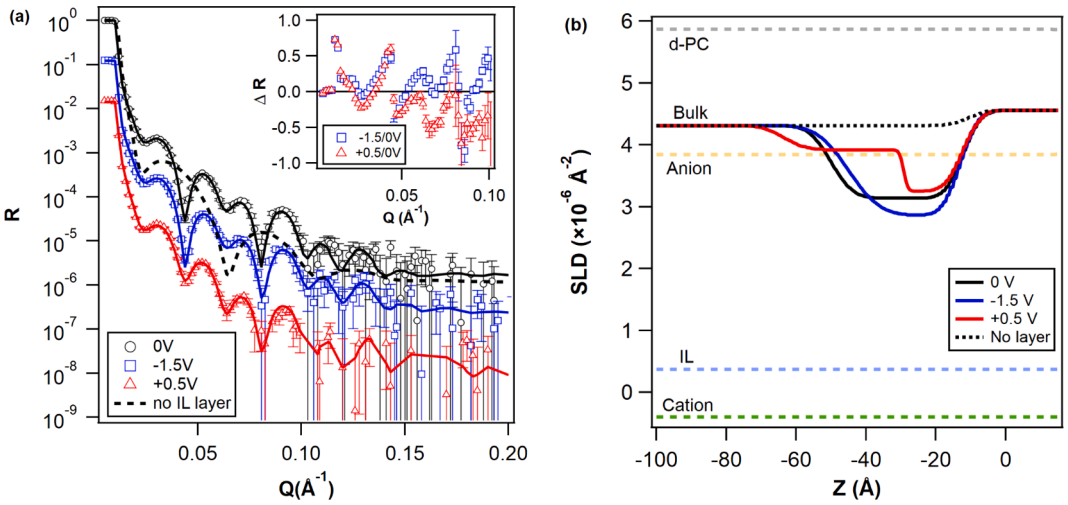

Fig. 8. (a) Experimental neutron reflectivity, R, of 20% w/w [$P_{6,6,6,14}$][BOB] in d-PC at the gold electrode surface for different applied potentials (applied order as indicated in the legend) as a function of the momentum transfer vector Q_z. The symbols show the experimental data, whilst the solid lines represent the simulated reflectivities obtained from the best fit to the data. For clarity, the curves have been offset on the y-axis. For comparison, the dashed line shows the predicted reflectivity for the same surface and solution without an interfacial IL layer. The inset shows asymmetry plots $\Delta R = \frac{[R^V(Q_z) - R^0(Q_z)]}{[R^V(Q_z) + R^0(Q_z)]}$, highlighting the difference of reflectivity between polarized potentials and 0 V. (b) Corresponding model SLD profiles obtained from the best fits to the reflectivity curves as a function of distance z, where the gold-solution interface is located at z = 0. Dashed lines represent the corresponding pure component SLDs.

different applied potentials, the thickness and average SLD of the interfacial region both vary. For 0 V and −1.5 V, a one-layer model is sufficient to capture the features of the reflectivity curves, and an additional layer model did not provide a noticeable improvement in fit quality (lower FOM). The two-layer model afforded a better fit for +0.5 V (cf. Figure S7), consisting of a significant SLD drop close to the electrode interface, followed by a broader layer with higher SLD. The specific parameters obtained from the fits (layer thickness, roughness, and SLD) can be found in the Supplementary Information (cf. Table S3). Overall, the SLD profiles demonstrate a broad interfacial region with relatively low SLDs for all the applied potentials, which can be attributed to increased ion density at the gold interface. Note that an unambiguous absolute composition cannot be extracted from the fits, due to an unknown solvent composition. However, the *changes* in composition can be easily followed. At 0 V, the boundary layer's relatively low SLD suggests a high cation concentration at the gold interface. The depth of this minimum is notably lower at the negative potential, indicating a surface enrichment of cations. Moreover, the slightly decreased thickness of the boundary layer at −1.5 V commensurates with a more well-defined, condensed cation layer at the interface, which is expected to counter the negative surface potential. The thickness of the layer under these conditions is also consistent with a bilayer structure. Upon reversing the potential bias to +0.5 V, the SLD profile shows a dramatic change. The depth of the minimum of the SLD increases. In addition, the SLD profile presents a significantly reduced thickness for the first layer, which is comparable with the [BOB]$^-$ anion's size at the positive potential. Together, these changes in the SLD profile can be inferred as an interfacial structure transition from the self-assembled bilayer cation domain to an anion-rich interfacial layer as suggested by our QCM data.

An estimation of interfacial SLD based on the change of "mass charge" from QCM data was applied to check the consistency of the two characterizations. To the best of the authors' knowledge, this has not been attempted before. The description of the conversion between mass change and mass "charge" change can be found in the Supplementary Information (cf. **Table S4**) and previous publication by N. Hjalmarsson et al. [37]. Briefly, the change in charge from QCM data could be used to calculate the number of counter ions needed to balance the electrode's charge within the applied potential. For simplicity, the ions are considered as spheres, and their occupied area is described by their largest cross-sectional area. Any electrode area not occupied by the counterions is assumed to be filled with ion pairs. PC is treated as "volume-free" because it could fill voids between and/or within ions. The ratio between the number of each species (*e.g.,* counterion, ion pair, d-PC as solvent molecule) can then be used to estimate what the SLD should be very coarsely. See the Supplementary Information for more details on the calculation and results (cf. **Table S5**).

From the QCM results, a relationship between inferred charge and voltage can be extracted. The surface charge at the applied potential of +0.5 V is estimated at 35.6 $\mu C/cm^2$. If this charge is balanced by anions layer, and the remaining space is assigned to ion pairs, then this results in a predicted SLD of 3.4 × 10^{-6} Å^{-2}, 3.6 × 10^{-6} Å^{-2}, or 3.8 × 10^{-6} Å^{-2}, assuming a deuterated solvent molar fraction of 0, 10% and 20%, respectively, inclusion of solvent results in an SLD higher than that actually measured, (owing to the high SLD of d-PC). The zero solvent predicted SLD, however, is remarkably close to that measured by NR (cf. Fig. 8 red line and value 3.25 × 10^{-6} Å^{-2}, in **Table S3**). This calculation in turn implies that, due to the very different ion volumes, the anion molar faction is 98%, consistent with a thin coulombically ordered layer that is mainly composed of anions. At the same time, and accepting the crudity of the model, this well-matched SLD prediction provides strong support for the contention of a smaller solvent effect for the [$P_{6,6,6,14}$][BOB]/PC system, implied by the QCM data (cf. Fig. 3 and Fig. 7).

4. Conclusions

The interfacial composition and structure of two novel, non-halogenated ionic liquids (ILs) (trihexyl(tetradecyl)phosphonium-bis(mandelato)borate, [$P_{6,6,6,14}$][BMB] and trihexyl(tetradecyl) phosphonium-bis(oxalato)borate, [$P_{6,6,6,14}$][BOB]) dissolved in a polar solvent (propylene carbonate, PC) have been studied as a function of potential. Both electro-responsivity of the polar solvent and the IL interfacial layer can be observed and measured, due to the very different time scales of their response. Changes in the quartz crystal microbalance (QCM) resonant frequency revealed the electro-response of PC as a pure polar liquid, and this effect was also demonstrated in the [$P_{6,6,6,14}$][BMB]/PC system, indicating a significant solvent component of the IL interfacial film due to the larger size of the [BMB]$^-$ anion. Meanwhile, the interfacial mass variations for [$P_{6,6,6,14}$][BMB]/PC may be ascribed to the density difference of exchanged ions as the IL interfacial film responds to different potentials.

By contrast, the $[P_{6,6,6,14}][BOB]$/PC showed a weaker solvent effect as the consequence of the higher dissociation of the IL and smaller structure of $[BOB]^-$ anion, leading to a lower overall solvent fraction. In addition, a hitherto unobserved phenomenon was revealed for this system, whereby the externally applied voltage triggered an abrupt interphase transition from a bilayer composed of $[P_{6,6,6,14}]^+$ cations to a coulombically ordered monolayer. This electro-responsive transition of the latter system at the electrified interface was also studied using neutron reflectivity (NR) as an independent approach to confirm this observation. The NR data clearly support the hypothesis of a sharp, "catastrophic" transition from a thicker bilayer structure to an anion-rich, thin interfacial layer at an intermediate positive potential. Finally, we demonstrate for the first time that the inferred mass changes from electro-responsive QCM can be translated directly into corresponding scattering length density (SLD) changes in neutron reflectance, opening a new route for characterizing electrified interfaces in IL systems.

The idea of interfacial self-assembly structures in ILs is not in itself new: the electric double layer (EDL) of pure ILs has been explored in depth with various advanced techniques [16,30,32,34,35], and also recently in polar solvents [47,49,58,64]. However, many of the ILs studied contain fluorine (FAILs), which can bring toxic and corrosive risks, particularly in environments where high pressures can be experienced. The response of self-assembly to potential is less well studied, particularly in solvents, and the interphase transition observed here is novel. This study may well explain some of the irreversible effects that appear to bedevil the community. It also provides the possibility of a "behavioural switch". Rather than the systematic response to the applied potential of the interfacial composition, and related properties such as friction coefficient [8,9,64], a threshold potential can be achieved at which the interphase transition leads to an abrupt change.

This study demonstrates that the interfacial structures of ILs can be modified as a function of applied potential, and the nature of the response to different polarities is strongly dependent on the nature and structure of the ionic species as well as solvent composition. It provides valuable molecular insight into the electro-tunability of IL boundary layers, which in future work for us and the field as a whole, will guide the development of future ionic liquid applications, and on the immediate horizon, the implementation of switch-based tribotronics and the design of IL-based multilayer supercapacitors.

CRediT authorship contribution statement

Sichao Li: Conceptualization, Investigation, Methodology, Visualization, Writing – original draft, Writing – review & editing, Formal analysis. **Georgia A. Pilkington:** Conceptualization, Methodology, Writing – review & editing, Supervision. **Filip Mehler:** Formal analysis, Visualization, Investigation, Writing – review & editing. **Oliver S. Hammond:** Investigation, Writing – review & editing. **Anthony Boudier:** Investigation, Writing – review & editing. **Alexei Vorobiev:** Resources. **Sergei Glavatskih:** Resources, Writing – review & editing, Project administration, Funding acquisition. **Mark W. Rutland:** Conceptualization, Funding acquisition, Investigation, Methodology, Project administration, Resources, Supervision, Writing – review & editing.

Declaration of Competing Interest

The authors declare that they have no known competing financial interests or personal relationships that could have appeared to influence the work reported in this paper.

Data availability

Data will be made available on request.

Acknowledgement

The authors thank the ILL for providing neutron beam time on SuperADAM (doi:10.5291/ILL-DATA.9-13-1006). The Knut and Alice Wallenberg Foundation (Project No. KAW2012.0078), the Swedish Research Council, VR (Project No. 2017-04080) and the Swedish Foundation for Strategic Research (Project No. EM16-0013, "REFIT") are acknowledged for their financial support. Prof. Oleg N. Antzutkin group (Luleå University of Technology) is gratefully acknowledged for providing the ILs.

Appendix A. Supplementary data

Supplementary data to this article can be found online at https://doi.org/10.1016/j.jcis.2023.08.111.

References

[1] T. Welton, Room-temperature ionic liquids, Solvents for synthesis and catalysis, Chemical reviews 99 (8) (1999) 2071–2084.
[2] F. Zhou, Y. Liang, W. Liu, Ionic liquid lubricants: designed chemistry for engineering applications, Chemical Society Reviews 38 (9) (2009) 2590–2599.
[3] D.R. MacFarlane, M. Forsyth, P.C. Howlett, M. Kar, S. Passerini, J.M. Pringle, H. Ohno, M. Watanabe, F. Yan, W. Zheng, Ionic liquids and their solid-state analogues as materials for energy generation and storage, Nature Reviews Materials 1 (2) (2016) 1–15.
[4] M. Watanabe, M.L. Thomas, S. Zhang, K. Ueno, T. Yasuda, K. Dokko, Application of ionic liquids to energy storage and conversion materials and devices, Chemical reviews 117 (10) (2017) 7190–7239.
[5] C. Ye, W. Liu, Y. Chen, L. Yu, Room-temperature ionic liquids: a novel versatile lubricant, Chemical Communications 21 (2001) 2244–2245.
[6] M. Radiom, Ionic liquid–solid interface and applications in lubrication and energy storage, Current Opinion in Colloid & Interface Science 39 (2019) 148–161.
[7] D.S. Silvester, R. Jamil, S. Doblinger, Y. Zhang, R. Atkin, H. Li, Electrical double layer structure in ionic liquids and its importance for supercapacitor, battery, sensing, and lubrication applications, The Journal of Physical Chemistry C 125 (25) (2021) 13707–13720.
[8] H. Li, M.W. Rutland, M. Watanabe, R. Atkin, Boundary layer friction of solvate ionic liquids as a function of potential, Faraday Discussions 199 (2017) 311–322.
[9] J. Sweeney, F. Hausen, R. Hayes, G.B. Webber, F. Endres, M.W. Rutland, R. Bennewitz, R. Atkin, Control of nanoscale friction on gold in an ionic liquid by a potential-dependent ionic lubricant layer, Physical review letters 109 (15) (2012), 155502.
[10] M. Cai, Q. Yu, W. Liu, F. Zhou, Ionic liquid lubricants: When chemistry meets tribology, Chemical Society Reviews 49 (21) (2020) 7753–7818.
[11] F.U. Shah, S. Glavatskih, O.N. Antzutkin, Boron in tribology: from borates to ionic liquids, Tribology letters 51 (3) (2013) 281–301.
[12] R.P. Swatloski, J.D. Holbrey, R.D. Rogers, Ionic liquids are not always green: hydrolysis of 1-butyl-3-methylimidazolium hexafluorophosphate, Green Chemistry 5 (4) (2003) 361–363.
[13] F.U. Shah, S. Glavatskih, D.R. MacFarlane, A. Somers, M. Forsyth, O.N. Antzutkin, Novel halogen-free chelated orthoborate–phosphonium ionic liquids: synthesis and tribophysical properties, Physical Chemistry Chemical Physics 13 (28) (2011) 12865–12873.
[14] M.R. Shimpi, P. Rohlmann, F.U. Shah, S. Glavatskih, O.N. Antzutkin, Transition anionic complex in trihexyl (tetradecyl) phosphonium-bis (oxalato) borate ionic liquid–revisited, Physical Chemistry Chemical Physics 23 (10) (2021) 6190–6203.
[15] P. Rohlmann, S. Watanabe, M.R. Shimpi, J. Leckner, M.W. Rutland, J.B. Harper, S. Glavatskih, Boundary lubricity of phosphonium bisoxalatoborate ionic liquids, Tribology International 161 (2021), 107075.
[16] A.B. Reddy, B. Munavirov, G.A. Pilkington, G. Calderon Salmeron, M.W. Rutland, S. Glavatskih, Micro-to nano-and from surface to bulk: Influence of halogen-free ionic liquid architecture and dissociation on green oil lubricity, ACS Sustainable Chemistry & Engineering. 9 (40) (2021) 13606–13617.
[17] P. Rohlmann, B. Munavirov, I. Furó, O. Antzutkin, M.W. Rutland, S. Glavatskih, Non-halogenated ionic liquid dramatically enhances tribological performance of biodegradable oils, Frontiers in chemistry 7 (2019) 98.
[18] B. Munavirov, J.J. Black, F.U. Shah, J. Leckner, M.W. Rutland, J.B. Harper, S. Glavatskih, The effect of anion architecture on the lubrication chemistry of phosphonium orthoborate ionic liquids, Scientific reports 11 (1) (2021) 1–16.
[19] R. Gusain, O.P. Khatri, Halogen-free ionic liquids: effect of chelated orthoborate anion structure on their lubrication properties, RSC Advances 5 (32) (2015) 25287–25294.
[20] Y. Lu, S. Watanabe, S. Sasaki, S. Glavatskih, Lubricity of chelated orthoborate-phosphonium ionic liquids on tetrahedral amorphous carbon and steel surfaces, Journal of Molecular Liquids 378 (2023), 121571.
[21] P. Rohlmann, J.J. Black, S. Watanabe, J. Leckner, M.R. Shimpi, M.W. Rutland, J. B. Harper, S. Glavatskih, Tribochemistry of imidazolium and phosphonium bis (oxalato) borate ionic liquids: understanding the differences, Tribology International 108263 (2023).

[22] S. Glavatskih, E. Höglund, Tribotronics—towards active tribology, Tribology international 41 (9–10) (2008) 934–939.
[23] M.V. Fedorov, A.A. Kornyshev, Ionic liquids at electrified interfaces, Chemical reviews 114 (5) (2014) 2978–3036.
[24] M.Z. Bazant, B.D. Storey, A.A. Kornyshev, Double layer in ionic liquids: Overscreening versus crowding, Physical review letters 106 (4) (2011), 046102.
[25] L.A. Jurado, R.M. Espinosa-Marzal, Insight into the electrical double layer of an ionic liquid on graphene, Scientific reports 7 (1) (2017) 1–12.
[26] M. Mezger, H. Schroder, H. Reichert, S. Schramm, J.S. Okasinski, S. Schoder, V. Honkimaki, M. Deutsch, B.M. Ocko, J. Ralston, Molecular layering of fluorinated ionic liquids at a charged sapphire (0001) surface, Science 322 (5900) (2008) 424–428.
[27] R. Hayes, G.G. Warr, R. Atkin, Structure and nanostructure in ionic liquids, Chemical reviews 115 (13) (2015) 6357–6426.
[28] Q. Zheng, Z.A. Goodwin, V. Gopalakrishnan, A.G. Hoane, M. Han, R. Zhang, N. Hawthorne, J.D. Batteas, A.A. Gewirth, R.M. Espinosa-Marzal, Water in the Electrical Double Layer of Ionic Liquids on Graphene, ACS Nano 17 (10) (2023) 9347–9360.
[29] Y.-L. Wang, B. Li, S. Sarman, F. Mocci, Z.-Y. Lu, J. Yuan, A. Laaksonen, M.D. Fayer, Microstructural and dynamical heterogeneities in ionic liquids, Chemical reviews 120 (13) (2020) 5798–5877.
[30] X. Mao, P. Brown, C. Červinka, G. Hazell, H. Li, Y. Ren, D. Chen, R. Atkin, J. Eastoe, I. Grillo, Self-assembled nanostructures in ionic liquids facilitate charge storage at electrified interfaces, Nature Materials 18 (12) (2019) 1350–1357.
[31] A.M. Smith, K.R. Lovelock, N.N. Gosvami, P. Licence, A. Dolan, T. Welton, S. Perkin, Monolayer to bilayer structural transition in confined pyrrolidinium-based ionic liquids, The journal of physical chemistry letters 4 (3) (2013) 378–382.
[32] S. Watanabe, G.A. Pilkington, A. Oleshkevych, P. Pedraz, M. Radiom, R. Welbourn, S. Glavatskih, M.W. Rutland, Interfacial structuring of non-halogenated imidazolium ionic liquids at charged surfaces: effect of alkyl chain length, Physical Chemistry Chemical Physics 22 (16) (2020) 8450–8460.
[33] M. Han, S.A. Rogers, R.M. Espinosa-Marzal, Rheological characteristics of ionic liquids under nanoconfinement, Langmuir 38 (9) (2022) 2961–2971.
[34] R. Atkin, N. Borisenko, M. Drüschler, S.Z. El Abedin, F. Endres, R. Hayes, B. Huber, B. Roling, An in situ STM/AFM and impedance spectroscopy study of the extremely pure 1-butyl-1-methylpyrrolidinium tris (pentafluoroethyl) trifluorophosphate/Au (111) interface: potential dependent solvation layers and the herringbone reconstruction, Physical Chemistry Chemical Physics 13 (15) (2011) 6849–6857.
[35] B. Roling, M. Drüschler, B. Huber, Slow and fast capacitive process taking place at the ionic liquid/electrode interface, Faraday discussions 154 (2012) 303–311.
[36] N. Hjalmarsson, D. Wallinder, S. Glavatskih, R. Atkin, T. Aastrup, M.W. Rutland, Weighing the surface charge of an ionic liquid, Nanoscale 7 (38) (2015) 16039–16045.
[37] N. Hjalmarsson, E. Bergendal, Y.-L. Wang, B. Munavirov, D. Wallinder, S. Glavatskih, T. Aastrup, R. Atkin, I. Furo, M.W. Rutland, Electro-responsive surface composition and kinetics of an ionic liquid in a polar oil, Langmuir 35 (48) (2019) 15692–15700.
[38] S. Zhou, K.S. Panse, M.H. Motevaselian, N.R. Aluru, Y. Zhang, Three-dimensional molecular mapping of ionic liquids at electrified interfaces, ACS nano 14 (12) (2020) 17515–17523.
[39] M. Radiom, P. Pedraz, G. Pilkington, P. Rohlmann, S. Glavatskih, M.W. Rutland, Anomalous interfacial structuring of a non-halogenated ionic liquid: effect of substrate and temperature, Colloids and Interfaces 2 (4) (2018) 60.
[40] O. Werzer, E.D. Cranston, G.G. Warr, R. Atkin, M.W. Rutland, Ionic liquid nanotribology: mica–silica interactions in ethylammonium nitrate, Physical Chemistry Chemical Physics 14 (15) (2012) 5147–5152.
[41] A. Elbourne, J. Sweeney, G.B. Webber, E.J. Wanless, G.G. Warr, M.W. Rutland, R. Atkin, Adsorbed and near-surface structure of ionic liquids determines nanoscale friction, Chemical Communications 49 (60) (2013) 6797–6799.
[42] R. Atkin, H. Li, J. Sweeney, A. Elbourne, G. Webber, M. Rutland, G.G. Warr, Effect of surface nanostructure and ion structure on the nanotribology of the graphite: Ionic liquid interface, Abstracts of Papers of the American Chemical Society (2014).
[43] M.A. Gebbie, M. Valtiner, X. Banquy, E.T. Fox, W.A. Henderson, J.N. Israelachvili, Ionic liquids behave as dilute electrolyte solutions, Proceedings of the National Academy of Sciences 110 (24) (2013) 9674–9679.
[44] M. Mezger, R. Roth, H. Schröder, P. Reichert, D. Pontoni, H. Reichert, Solid-liquid interfaces of ionic liquid solutions—Interfacial layering and bulk correlations, The Journal of chemical physics 142 (16) (2015), 164707.
[45] O.S. Hammond, G. Bousrez, F. Mehler, S. Li, M.R. Shimpi, J. Doutch, L. Cavalcanti, S. Glavatskih, O.N. Antzutkin, M.W. Rutland, Molecular architecture effects on bulk nanostructure in bis (Orthoborate) ionic liquids, Small 2300912 (2023).
[46] P.K. Cooper, H. Li, N.R. Yepuri, A. Nelson, G.B. Webber, A.P. Le Brun, T. A. Darwish, G.G. Warr, R. Atkin, Ionic liquid adsorption at the silica–oil interface revealed by neutron reflectometry, The Journal of Physical Chemistry C 122 (42) (2018) 24077–24084.
[47] G.A. Pilkington, K. Harris, E. Bergendal, A.B. Reddy, G.K. Palsson, A. Vorobiev, O. N. Antzutkin, S. Glavatskih, M.W. Rutland, Electro-responsivity of ionic liquid boundary layers in a polar solvent revealed by neutron reflectance, The Journal of Chemical Physics 148 (19) (2018), 193806.
[48] Y.-L. Wang, M. Golets, B. Li, S. Sarman, A. Laaksonen, Interfacial structures of trihexyltetradecylphosphonium-bis (mandelato) borate ionic liquid confined between gold electrodes, ACS Applied Materials & Interfaces 9 (5) (2017) 4976–4987.
[49] G.A. Pilkington, A. Oleshkevych, P. Pedraz, S. Watanabe, M. Radiom, A.B. Reddy, A. Vorobiev, S. Glavatskih, M.W. Rutland, Electroresponsive structuring and friction of a non-halogenated ionic liquid in a polar solvent: effect of concentration, Physical Chemistry Chemical Physics 22 (34) (2020) 19162–19171.
[50] A.B. Reddy, G.A. Pilkington, M.W. Rutland, S. Glavatskih, Tribotronic control of an ionic boundary layer in operando extends the limits of lubrication, Scientific Reports 12 (1) (2022) 20479.
[51] G. Sauerbrey, Verwendung von Schwingquarzen zur Wägung dünner Schichten und zur Mikrowägung, Zeitschrift für physik 155 (2) (1959) 206–222.
[52] A. Devishvili, K. Zhernenkov, A.J. Dennison, B. Toperverg, M. Wolff, B. Hjörvarsson, H. Zabel, SuperADAM: Upgraded polarized neutron reflectometer at the Institut Laue-Langevin, Review of Scientific Instruments 84 (2) (2013), 025112.
[53] M. Björck, G. Andersson, GenX: an extensible X-ray reflectivity refinement program utilizing differential evolution, Journal of Applied Crystallography 40 (6) (2007) 1174–1178.
[54] A. Glavic, M. Björck, GenX 3: the latest generation of an established tool, Journal of applied crystallography 55 (4) (2022).
[55] A. Nelson, Co-refinement of multiple-contrast neutron/X-ray reflectivity data using MOTOFIT, Journal of applied crystallography 39 (2) (2006) 273–276.
[56] M. Born, E. Wolf, Principles of optics: electromagnetic theory of propagation, interference and diffraction of light, Elsevier, 2013.
[57] D. Wakeham, A. Nelson, G.G. Warr, R. Atkin, Probing the protic ionic liquid surface using X-ray reflectivity, Physical Chemistry Chemical Physics 13 (46) (2011) 20828–20835.
[58] G.A. Pilkington, R. Welbourn, A. Oleshkevych, S. Watanabe, P. Pedraz, M. Radiom, S. Glavatskih, M.W. Rutland, Effect of water on the electroresponsive structuring and friction in dilute and concentrated ionic liquid lubricant mixtures, Physical Chemistry Chemical Physics 22 (48) (2020) 28191–28201.
[59] S. Bruckenstein, M. Shay, Experimental aspects of use of the quartz crystal microbalance in solution, Electrochimica Acta 30 (10) (1985) 1295–1300.
[60] S. Li, P. Zhang, F.F. Pasquale, C.H. Patrick, G. Feng, S. Dai, T.C. Peter, Enhanced performance of dicationic ionic liquid electrolytes by organic solvents, Journal of Physics: Condensed Matter 26 (28) (2014), 284105.
[61] A.M. Smith, K.R. Lovelock, S. Perkin, Monolayer and bilayer structures in ionic liquids and their mixtures confined to nano-films, Faraday discussions 167 (2013) 279–292.
[62] A.M. Smith, M.A. Parkes, S. Perkin, Molecular friction mechanisms across nanofilms of a bilayer-forming ionic liquid, The journal of physical chemistry letters 5 (22) (2014) 4032–4037.
[63] M. Han, H. Kim, C. Leal, M. Negrito, J.D. Batteas, R.M. Espinosa-Marzal, Insight into the electrical double layer of ionic liquids revealed through its temporal evolution, Advanced Materials Interfaces 7 (24) (2020) 2001313.
[64] S.W. Coles, A.M. Smith, M.V. Fedorov, F. Hausen, S. Perkin, Interfacial structure and structural forces in mixtures of ionic liquid with a polar solvent, Faraday discussions 206 (2018) 427–442.